



Università di Pisa

---

DIPARTIMENTO DI FISICA "ENRICO FERMI"

Corso di Laurea in Fisica

TESI DI LAUREA

## Commissioning and first data analysis of the Mainz radius experiment.

Candidato:

**Adriano Del Vincio**

Matricola 562946

Relatore:

**Prof. Francesco Forti**

**Prof.ssa Concettina Sfienti**

# Contents

<b>1</b>	<b>Introduction</b>	<b>2</b>
1.1	Neutron skin thickness and EOS . . . . .	2
1.2	Parity-violating scattering experiment . . . . .	2
1.3	Transverse asymmetry . . . . .	2
1.3.1	Motivation . . . . .	2
1.3.2	Conventions used . . . . .	2
<b>2</b>	<b>Transverse Asymmetry</b>	<b>3</b>
2.1	Description of the process . . . . .	3
2.1.1	Elastic scattering . . . . .	3
2.1.2	Inelastic scattering . . . . .	3
2.1.3	Model description . . . . .	3
2.2	State of the Experiment . . . . .	3
<b>3</b>	<b>Experimental setup</b>	<b>4</b>
3.1	First description of the experiment . . . . .	4
3.2	Mami . . . . .	4
3.2.1	Acceleration stage . . . . .	4
3.2.2	Polarized Beam . . . . .	4
3.2.3	Mott, Compton and Moller polarimenters . . . . .	5
3.3	A1 spectrometers hall . . . . .	6
3.4	Detectors and beam monitors . . . . .	7
3.4.1	Detectors A and B . . . . .	7
3.4.2	Monitors and stabilization . . . . .	7
3.5	Electronics . . . . .	7
3.5.1	VFCs . . . . .	7
3.5.2	Nino board . . . . .	8
3.5.3	Master Board . . . . .	8
<b>4</b>	<b>Test and beam time analysis</b>	<b>10</b>
4.1	Model for fitting the data . . . . .	10
4.2	Data tree . . . . .	10
4.3	Detectors test . . . . .	10
4.3.1	Rate of Cosmic rays . . . . .	11
4.4	Analysis . . . . .	11
4.4.1	Alignment of the scattering plane . . . . .	11
4.4.2	Calibration of the VFCs monitors . . . . .	11
4.4.3	Calibration of the PIMO monitors . . . . .	11
4.4.4	Current and ENMO monitors . . . . .	12
4.4.5	Calibration of the pmts . . . . .	14
4.4.6	Rates on lead . . . . .	16
4.5	Asymmetry on Carbon . . . . .	16
4.5.1	Autocalibration procedure . . . . .	16
4.5.2	least square fit . . . . .	16
4.5.3	False asymmetries . . . . .	20
4.5.4	?Bootstrap?? . . . . .	21
4.5.5	?interval estimation?? . . . . .	21
<b>5</b>	<b>Conclusion and outlook</b>	<b>22</b>

<b>Appendices</b>	<b>23</b>
<b>A Some Appendix</b>	<b>24</b>

### **Abstract**

short introduction

# Chapter 1

## Introduction

- explain neutron skin thickness.
- connection to neutron stars radius, and neutron stars description.
- Equation of state (EoS) for high density nuclear matter.
- Parity-violating scattering experiment for extracting neutron skin thickness.
- mention the weak form factor.
- Transverse asymmetry as background for Parity-violating experiment.
- Mention the other experiment, like PREX, that measure zero  $A_n$  for Lead.

### 1.1 Neutron skin thickness and EOS

In this section we have to explain what is the neutron skin thickness and why this parameter is related to the Equation of State for nuclear matter (in particular, the slope of the Symmetry energy in the semiempirical mass formula). Then, explain the parallelism between Neutron stars and Nuclear matter (they share the same EOS), and underline the relation between radius of the neutron stars and EOS.

### 1.2 Parity-violating scattering experiment

This section is for describing the way it's possible to extract the neutron skin thickness. Here I have to mention the weak form factor and the important fact that the neutrons are more important than the protons in the parity-violating scattering, because of the weak mixing angle.

### 1.3 Transverse asymmetry

Here we have to introduce the aim of this thesis: the transverse asymmetry is a source of background for the parity-violating experiments. Furthermore the theory is not working well for some nuclei ( $^{208}Pb$ ), so mention PREX paper about the last measurement on carbon and lead, the problem that they measure 0 transverse asymmetry.

#### 1.3.1 Motivation

Here present all the motivation for this thesis, so the fact that we want to measure the rates on lead for the future experiment, test the new electronics, measure another time the transverse asymmetry on  $^{12}C$

#### 1.3.2 Conventions used

It could be useful, here, to have a subsection to explain the terminology for this thesis, to avoid misunderstanding.

# Chapter 2

## Transverse Asymmetry

- Physics behind the  $A_n$  asymmetry, dependence on  $Q^2$ , the formula  $\frac{\sigma_{\uparrow} - \sigma_{\downarrow}}{\sigma_{\uparrow} + \sigma_{\downarrow}}$
- state of the art of the Exp.
- Model description: so scattering amplitude, theoretical prediction
- Expected error  $\delta A_t$
- open question: problems with lead, dependence of  $E_{beam}$ , dependence from Z, Z/A

### 2.1 Description of the process

Explain the scattering process we are studying (at least one figure to visualize the kinematics of the scattering). Mention the link between this process and time-reversal operator. Add two figures for elastic and inelastic scattering.

#### 2.1.1 Elastic scattering

Write the amplitude for the elastic (how to manipulate expression, maybe in the appendix).

#### 2.1.2 Inelastic scattering

Explain how it's possible to compute the inelastic expression, what kind of approximations are used (optical theorem...)

#### 2.1.3 Model description

Present the theoretical formula for the Transverse asymmetry, and comment on energy, Z, Z/A dependencies

### 2.2 State of the Experiment

Write down the formula  $\frac{\sigma_{\uparrow} - \sigma_{\downarrow}}{\sigma_{\uparrow} + \sigma_{\downarrow}}$ . Hints at how to measure the Transverse asymmetry (remember to mention we have a polarized beam against a unpolarized target). Explain the expected error for the reconstructed asymmetry. Furthemore talk about the last mesurements obtained by the other collaborations, an outlook of the current situation. Maybe add also how we proceed to measure the transverse asymmetry, so the structure of the event, polarities patterns...

# Chapter 3

## Experimental setup

- description of MAMI, how the beam is produced, how the electrons are polarized.
- description of A1.
- description of beam stabilization, how the monitors measure the beam parameters.
- Electronics description, DAQ system, VFC monitors.
- Detectors A and B.

### 3.1 First description of the experiment

**First description of the experiment, how we want to collect data, new picture of the kinematic of the experiment. Maybe here it's a good point to describe the structure of the event.** To measure the Beam-Normal single spin asymmetry, a polarized beam of 570 MeV will be sent against a 10 mm  $^{12}C$  target. The detectors consist of two fused-silica coupled to 3 (detector B) and 8 (detector A) pmts, which collect the Cherenkov light emitted when an electron pass through the fused-silica. The detector are placed inside the two spectrometer of the A1 hall, which are not used in this experiment due to the high luminosity of the beam ( $20\mu A$ ) that is away from their good point of operation.

The photomultipliers asymmetry due the change of the electrons spin is the target of the measurement. The pmts signals are collected and digitalized by the **NINO** board, after a threshold selection, and sent to the A1 control room computer, where the DAQ program collect the data together with all the data coming from the Beam monitors producing Binary files, which are later analyzed by the analysis program, which is significant part of the work done in the framework of the thesis.

The data collected are divided in *Events* made by 4 *sub-events* in sequence. Each event correspond to a temporal window of  $\simeq 80\mu s$ , where each sub-event is  $20\mu s$  long. Here it's important to clarify that unlike the majority of experiments in high energy physics, an event is made by all the electrons interacting with the detectors during the time interval of the event, and we will refer to this hereafter unless otherwise stated. The division into sub-events reflects the polarization sequence of the beam. The PMTS counts and the beam monitor values are saved for each subevent, along with the time length of the event and other values which are required to process beam monitor data.

### 3.2 Mami

How Mami produces polarized electron and how the particle are accelerated (the way Mainz Mikroton is working is completely different from the other accelerators, so maybe this section will be too long).

#### 3.2.1 Acceleration stage

explain how electrons are accelerated, and sent to different experiments.

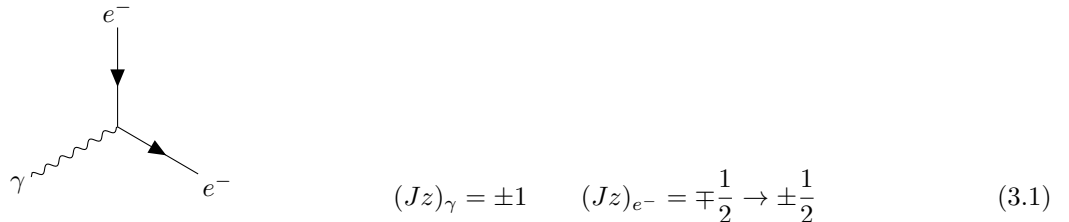
#### 3.2.2 Polarized Beam

Here a subsection to explain how the polarized electrons are produced. Important to mention the systematic error for the polarization mesurement (in our beam time we couldn't measure with Moller polarimeter, so this discussion is important for future experiment, however it's important

to say something about it). Remember to explain how the spin are rotated to the transverse plane, and the  $\frac{\lambda}{2}$

For the beam-normal single spin asymmetry a vertical polarized beam is necessary. At the MAMI electron accelerator is possible to produce a vertical polarized beam with energy in the range 180 MeV – 855 MeV [2]. In this section the procedure to orient the beam vertically, following an explanation of how the degree of polarization of the beam is measured.

The electron source used at MAMI is made by a strained GaAs/GaAsP superlattice photocathode illuminated by circular polarized light. A Pockels cell changes the helicity of the photons impinging on the electrons. The extracted electron has the same helicity of the incoming photon, let's suppose as an example:



$$(Jz)_\gamma = \pm 1 \quad (Jz)_{e^-} = \mp \frac{1}{2} \rightarrow \pm \frac{1}{2} \quad (3.1)$$

With the fast change of the Pockels cell it is possible to alternately revert the sign of the polarization. By the insertion of a  $\lambda/2$  plate between the laser system and the photocathode the polarization orientation of the electron beam can be reversed for each sub-event, useful later for the estimation of systematic errors. The beam polarization achieved with this source is roughly 80%, for the beam time it was : 0.79%

To switch from longitudinal polarization to transverse polarization, two devices are used: the **Wien filter** and a **double solenoid** located in the injection beam line.

*bird's eye view*

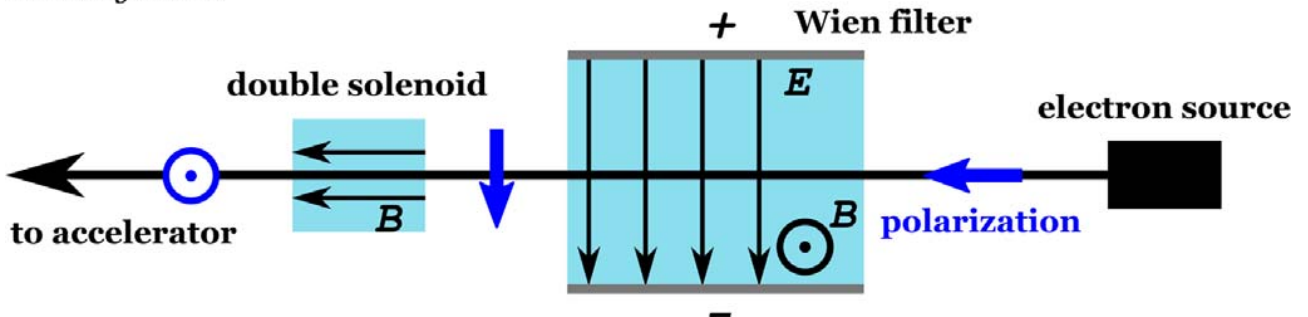


Figure 3.1: Setup for the trasverse polarization.

Following the picture, the longitudinal polarized electron from the source are rotated first in the XY plane, to obtain the transverse polarization, then with subsequent double solenoid the spins are rotate in the vertical direction. After this allignment the electrons go through the accelerator to the experimental hall. The spins then precesses during this time in the magnetic fields of the accelerator's bending magnets, following the BMT equation. In our experiment, because of the vertical polarization, only the residual horizontal component precedes during the motion. For conventional experiment the polarization vector is rotated by the Wien filter with an angle such that the polarization si longitudinally aligned in the experimental hall, considering that after the rotation, the polarization is affected by another rotation due to the spin precession. The rotation angles of the polarization vector through the accelerator are known from simulations and are also directly measured for relevant energies, for a beam of 570 MeV the rotation angle is  $55^\circ$  with an accuracy of  $\pm 2^\circ$ . At the beginning MAMI was not developed with the aim a trasverse beam. So it's not possible to measure directly the polarization for the vertical axis. However it's possible, with the existing setup, to exstimate the degree of polarization. For this purpose a Moller, Compton and Mott polarimeters are used. The vertical polarization alignment can be accomplished by the minimization of the horizontal components.

### 3.2.3 Mott, Compton and Moller polarimenters

Briefly explain how the Mott polarimeter works, for measuring the polarization of the beam.

To Measure the polarization of an electron beam different polarimeters can be used. Here we explain briefly the physics underlying the *Mott* polarimeter, used in the experiment. Consider an electron beam that is sent

towards a nucleus of charge  $Ze$ . We know from theory that the spin of the incident electron is affected by the electromagnetic field produced by the nucleus. This can be described as:

$$\vec{B}_{nucleus} = \frac{-1}{c} \vec{v} \times \vec{E}_{nucleus} = \frac{Ze}{mcr^3} \vec{L}$$

$$V = -\mu \cdot B_{nucleus} = \frac{Ze}{mcr^3} \vec{L} \cdot \vec{S}_{e^-}$$

We can recognize the spin-orbit interaction here. This term yields the polarization dependence of the cross section. The cross section can be model in the following way

$$\sigma(\theta) = I(\theta)[1 + S(\theta)\vec{P} \cdot \vec{n}]$$

Here a scheme to identify the scattering process:

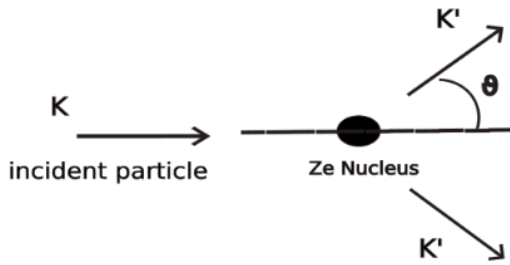


Figure 3.2: Scheme of the Mott scattering, the polarization is orthogonal to the plane,  $\vec{n} = \frac{\vec{k} \times \vec{k}'}{|\vec{k} \times \vec{k}'|}$

The direction of  $\vec{n}$  dependso on whether scattering to the left or right is being considered. Let's suppose our initial beam has a polarization  $P$ , and so we compute the asymmetry  $A(\theta)$  of the scattered electrons between left ( $N_L$ ) and right ( $N_R$ ).  $N_L$  and right  $N_R$  will be proportional respectively:

$$N_L = N_\downarrow[1 + S(\theta)] + N_\uparrow[1 - S(\theta)]$$

$$N_R = N_\uparrow[1 + S(\theta)] + N_\downarrow[1 - S(\theta)]$$

$$A(\theta) = \frac{N_L - N_R}{N_L + N_R} = \frac{N_\downarrow(1 + S(\theta)) + N_\uparrow(1 - S(\theta)) - N_\uparrow(1 + S(\theta)) + N_\downarrow(1 - S(\theta))}{N_L + N_R} = \dots = P \cdot S(\theta)$$

From the last equation we have a relation which give the beam polarization in terms of  $A(\theta)$  (which is what is measured) and the asymmetry function  $S(\theta)$  (known also as Sherman function). There are several calculation of the Sherman function, which is well-known for high energy electron scattering.

The total beam polarization is measured by a Moller polarimeter, in the experimental hall, with the beam polarization oriented longitudinally in the experimental hall. The Moller polarimeter can measure the longitudinal polarization of the beam. The other two polarimeters, Compton and Mott, located behind the injector linear accelerator (ILAC), are sensitive to the longitudinal and the trasverse horizontal components of the beam (with an energy around 3,5 MeV at this stage). The procedure for the allignment is the following: at the beginning of the beam time the Mott polarimeter is used for different settings of the solenoidal field, with the Wien filter angle equal (nominal) to 90°. The aim is to minimize the horizontal polarization component after the rotation performed by the double solenoid, changing the solenoidal magnetic field. Then a second optimization follows, using the Moller polarimeter for different Wien filter angles is performed. With the new Wien filter settings, another measurement is performed with the Mott polarimeter.

### 3.3 A1 spectrometers hall

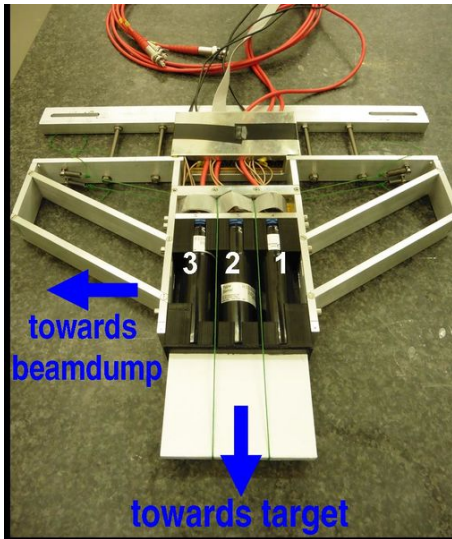
Describing the A1 room, how the spectrometers are operating (+ figures), a picture of the target and the important parameters, like thickness. Also mention the convention to use target with10% of the radiation lenght, to avoid double scattering. Mention that we need the Wobbler magnet to change the hitting position of the beam to prevent the target from melting. Then add a picture of the beam-line.

## 3.4 Detectors and beam monitors

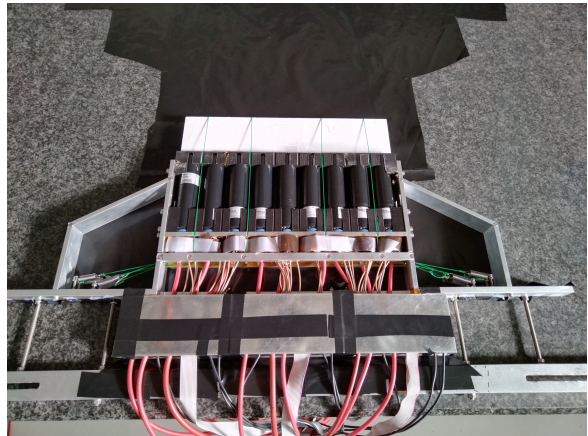
### 3.4.1 Detectors A and B

Describe the two detectors we placed inside the spectrometers, the  $Q^2$  for our measurement. The way the counts are collected, so the expected signal for the Čerenkov detector. Explain also how we will use the old detectors of the two spectrometers to align the elastic scattering plane to our detectors.

The scattered electrons that hit the target are detected via two fused-silica coupled with 3 PMTs and 8 PMTs. The electrons that pass through the fused-silica (refractive index 1.45) emits Čerenkov light that is detected by the PMTs. In the old electronic setup all the current generated by the pulse signal was collected, for each time interval of a sub-event. Then the asymmetry was reconstructed from the integrated current. This method is affected by high noise, and can't be applied for future experiments involving lead target. With the new electronic, all the single electron are counted, in order to work with the low rate expected from lead.



(a) *Detector B*



(b) *Detector A*

The fused silica size for detector B is (7 cm, 10 cm). Knowing that the expected number of event for cosmic rays is about  $1 \frac{\text{event}}{\text{m}^2 \text{s}}$

### 3.4.2 Monitors and stabilization

Explain how the monitors for the beam parameters work. (this section could be long, however the way these parameters are measured is particular, so it's important to explain everything properly).

## 3.5 Electronics

Short introduction about the old electronics setup and why a new version is needed, then describe all the electronics used for our experiment:

- Nino board for collecting the data from the PMTs
- VFCs for collecting the data from X21, X25, Y21, Y25, ENMO, I21, I13
- master board for collecting the monitors data/controlling the source/wobbler magnets.
- small boxes for switching from new electronic read-out to the old electronics read-out (spectrometers DAQ)

### 3.5.1 VFCs

Some parameters which describe the beam are needed in order to take into account possible effect in the measure of the Transverse asymmetry. The relevant data are the position in the  $(x, y)$  plane, the incident angles on the target, the current and energy of the beam. All these values are collected using the already existing monitors.

To collect the data from the monitors, single and multichannel, synchronous voltage-to-frequency converters (AD7742) are used. This devices contain an analog modulator that is able to convert the input voltage into an output pulse train, whose frequency is proportional to the input voltage.

The VFCs are powerd with an external tension of 5 V, and a differential voltage input in the range ( $-V_{ref}$ ,  $V_{ref}$ ) is also applied. An external clock signal, that is indicated with "CLKIN" is provived as a reference signal for the oscillator frequency. The analog input signal is sampled with by a switched capacitor, with a rate that is controlled by clock that can be supplied externally, in our case we used a 6 MHz. A scheme of the electronic circuit is drawn here (*aggiungere figura*), the output of the Comparator is a fixed width pulse (the pulse is initiated by the edge of the clock signal) with a frequency that goes from  $0.5\% \cdot f_{CLKIN}$  to  $0.45\% \cdot f_{CLKIN}$  [1], where the first correspond to 0,0 V in input and the second to  $V_{ref}$ . Neglecting possible systematic errors, the relation the output frequency and the input voltage is the following:

$$V_{in} = \frac{V_{ref}}{40\% \cdot f_{CLKIN}} (f_{out} - 5\% f_{CLKIN}) \quad (3.2)$$

We control the  $f_{CLKIN}$  with the period of the clock. The data are acquired counting the number of pulses that come from the comparator, so we can substitute to  $f$  the number of pulses (the two quantities are proportional), and we end with:

$$V_{in} = V_{ref} [2 \cdot \frac{N_{pulses} - 5\% N_{CLKN}}{40\% N_{CLKN}} - 1] \quad (3.3)$$

### 3.5.2 Nino board

The NINO board is our data acquisition system for the pmt counts. It is made by 32 analog input channels and it's power with  $\pm 5$  V. Each channel has an attenuator, and the signal pass through that before going to the Comparator, which compare the signal to the threshold. The Output signal is a Low-voltage differential signaling (LVDS). Each comparator can handle eight channel and for each of them it is possible to define a global threshold. With the current settings of NINO board, it is possible to change the threshold of each channel acting on another value, the attenuation, which decreases the value of the global threshold of each single channel. All the value that can be modified are 12 bit numbers, so a setting interval of (0.; 4095).

Two Nino board are used in the experiment, one for detector A and one for detector B. In principle it is possible to use only 8 and 3 of the 32 channels the are ready to use, considering we have only 3 and 8 pmts to read out. However it is useful to split the analog output signal by the pmts and send it to 4 different channels. So, working with the attenuation value, we can define 4 different threshold values for each pmt. This is something that can improve the noise management. This will be implemented for the future experiments, nevertheless this was not done during our data collection. The way we selected the threshold is explained in the following chapter (Analysis).

### 3.5.3 Master Board

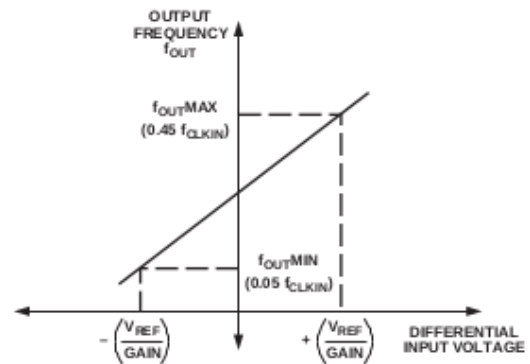


Figure 3.3: Frequency versus Voltage

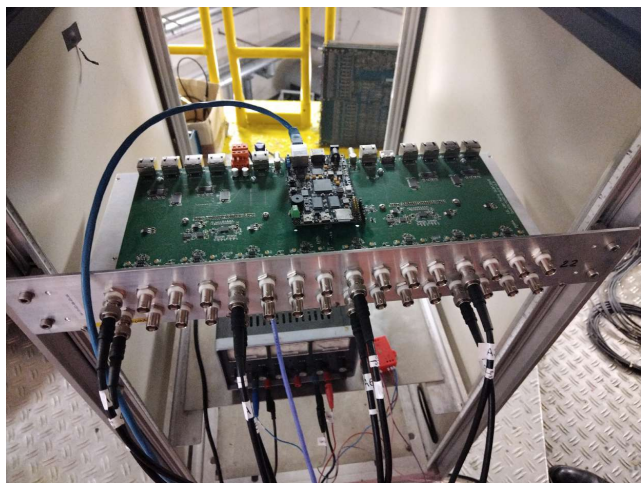


Figure 3.4: Nino Board

# Chapter 4

## Test and beam time analysis

1. development of the analysis program (description of the Levenberg-Marquardt-Algorithmus).
2. testing the analysis program with montecarlo data.
3. Test of the detectors in the Lab.
4. Beam line description.
5. Data Analysis
  - (a) thresholds scan
  - (b) Rates on  $Pb^{208}$ .
  - (c) Beam related asymmetry correction.
  - (d)  $C^{12}$  Asymmetry.

### 4.1 Model for fitting the data

Here I have to explain the model used for describing the data, so the problem of the false asymmetry induced by variations in beam position, angle, current and energy. Here is a good point to explain the De Bruijn sequence for the polarity patterns

### 4.2 Data tree

Explain how we compute all the values for the data tree, the position of the beam on the target, the angle, the correlated-difference values...

### 4.3 Detectors test

**Explain the test of the two detectors in the lab, how we select the threshold, the correlation of the pmts and coincidence to select the threshold. Mention also that we observed two knees in the plot of counts vs. attenuation.**

The Nino board, which digitizes the signal from the PMTS, has two parameters which can be used to select the internal threshold of the discriminator, to cut the low amplitude signals and can be adjusted changing the settings of the DAQ program. These two parameters are *Threshold* and *Attenuation*. *Threshold* means directly the charge value necessary for an impulse certain shape to be accepted by the signal discriminators. However the "physical" threshold can be also modified changing the *attenuation*. The relation between threshold and attenuation is not linear, but follows:

For our purposes, we select a common threshold values for all the pmts, and we decided to change only the attenuation values.

Before the Beam time, some test of the two detector were performed, to check that the pmts were still working and that the new electronic was able to count properly the pulses and store the data. For this studies, we didn't have a radioactive sources that we could use, so we moved the two detectors in the workshop of the accelerator, using the cosmic ray as a probe.

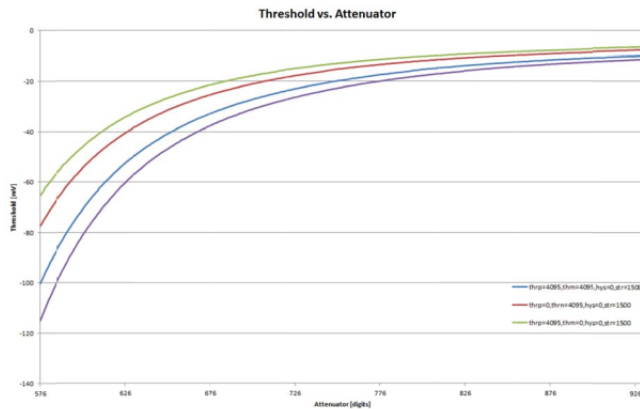


Figure 4.1: Threshold dependence against attenuation

#### 4.3.1 Rate of Cosmic rays

### 4.4 Analysis

One of the main goal for this experiment was to measure the well known trasverse asymmetry of  $^{12}C$ , already measured before, as a test for the new electronic system. Previous measurements of the Transverse asymmetry have been performed for a carbon target. For this beam-time, the two spektrometers were placed at an angle such that the  $Q^2$  values of the scattered electron is:

<i>SpektrometerA :</i>	$Q^2 = 0,041\,337 \text{ GeV}$	without Cut
<i>SpektrometerA :</i>	$Q^2 = 0,039\,451\,3 \text{ GeV}$	with Cut
<i>SpektrometerB :</i>	$Q^2 = 0,040\,477\,1 \text{ GeV}$	without Cut
<i>SpektrometerB :</i>	$Q^2 = 0,040\,584\,3 \text{ GeV}$	with Cut

The  $Q^2$  values is the same of the last measurement performed at MAMI, and is measured with and without rejecting the inelastic electrons.

#### 4.4.1 Alignment of the scattering plane

#### 4.4.2 Calibration of the VFCs monitors

Maybe it's important to divide this sections in two different part: the first part where I explain the Vfc convert the input voltage signal to a digital signal. In the second part just mention how we tuned the resistences (for X,Y monitors directly at the output signal with the oscilloscope, while for I21 and I13 monitors we used the data, so I'm able to produce plots only for the second ones).

#### 4.4.3 Calibration of the PIMO monitors

For the calibration of the X Y monitors, we used two target made by three carbon wires at a certain distance from each other, aligned horizontaly and vertically. The distance between the two center of the external wires is  $d_{horizontal} = 2,38 \text{ mm}$  for the target alligned horizontally and  $d_{vertical} = 2,33 \text{ mm}$  for the other one. When the horizontal wires target is cetered, we turn on the beam, and we take some data slowly changing the horizontal beam direction. The beam direction is changed by MAMI operators, varying the Magnetic field of the *Wobbler 16* magnets (4.2):

Then we repeat the same procedure with the other target, for the vertical direction. We observe that the pmts counts increase to a maximum, that is reached when the beam spot is centered on the carbon wire, and then decrease until the next carbon wire is hit by the beam.

We plot the pmt data *versus* the  $X25, X21, Y25, Y21$ , given in V. Given that we know the real distance between the two external wires, we can obtain the correct scaling factors to calculate the X and Y position values of the beam. To identify the three peaks in of the carbon target, we fit the data using a gaussian model (see 4.3). The mean  $\mu$  represents the center of the wire, given in V. Looking at the Beam line, we assume that the beam travels in a straight line. Let's consider the *Wobbler 16* magnet the "0" of a coordinate system, with the  $z$  axis

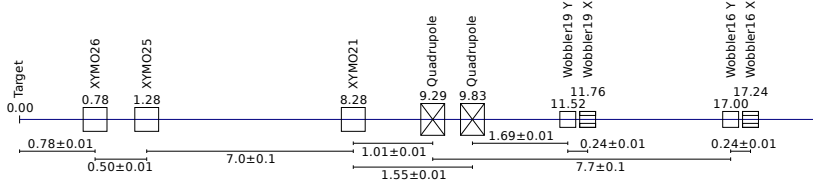


Figure 4.2: Beam line scheme.

pointing to the target (left direction in the beam scheme). The Beam parameters are measured by the Monitors  $X/Y_{21}$ ,  $X/Y_{25}$ , which are located at some distance respect to the target. Suppose we are working only with the  $Y_{25}$  monitor (the procedure is the same for the others). The Beam  $y$  position is described by:

$$y_{beam} = m \cdot (z - z_{wobbler16})$$

In the scheme 4.2 we easily compute the distance between the  $Y_{25}$  monitor and the *wobbler 16* magnet, so we have the slope  $m$ . The Position on the target is given by  $Y_{target} = m \cdot Z_{target}$ . With these simple equations then:

$$c_{Y25} = \frac{d_{vertical}[\text{mm}]}{Y_{target}} \quad (4.1)$$

$c_{Y25}$  indicates the scaling factor of the monitor. With these values the Analysis program compute the correct beam position, and from that the incident angles in the  $x, y$  directions, which are needed later for the analysis.

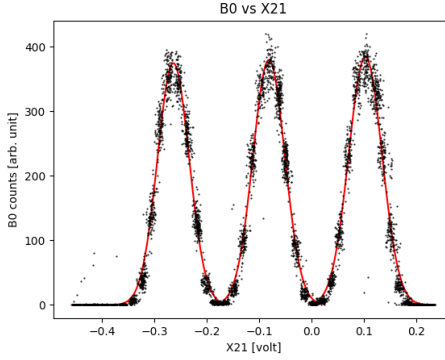


Figure 4.3: •

All this procedure can be easily checked if we plot now the  $X$  and  $Y$  position for the same two runs of data acquired with the wires. After placing the scaling factors obtained in the standard configuration file, we run the analysis another time and the physical values were computed 4.4

#### 4.4.4 Current and ENMO monitors

For the current monitors I13 and I21, we perform the calibration changing the current of the beam and observing the output values of the monitors (Voltage values). Then we perform a fit (for the beam current, we used the

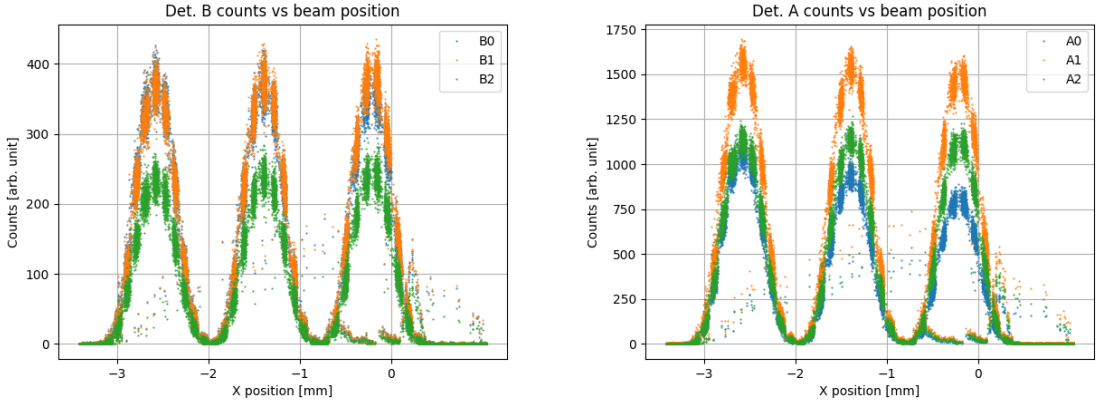


Figure 4.4: plot of the pmt Count against the physical values computed by the analysis program. Now the position of the three peaks correspond to the expected values measured for the target.

nominal values that we communicate to MAMI, has the values for the x-axis).

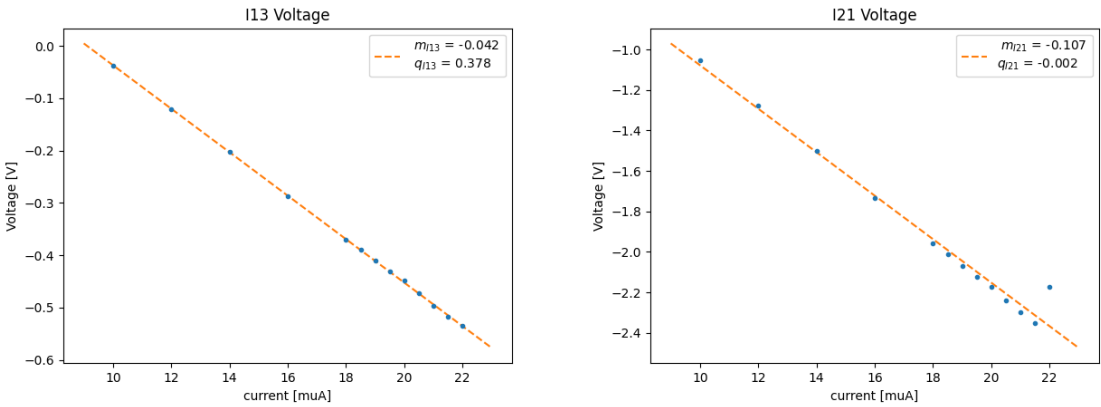


Figure 4.5: •

For the two monitors we are able to compute the offset and scale factor:

$$I_{13}^{volt} = m_{13} \cdot I_{13}^{Nom} + q_{13} \quad (4.2)$$

$$c_{13} = \frac{1}{m} \quad \text{offset} = -\frac{q_{13}}{m}$$

The same formula for current monitor I21.

The Enmo calibration is performed in a different way from the other monitors. The polarity signal is sent to MAMI, and they produce a signal for the ENMO that somehow (need to investigate exactly how they do that) shows a difference between the first two subevents and the last two. This difference is equal (nominal) to 22,6 keV. The idea now is to produce an histogram for the quantity  $\delta E$  (with  $E_{18}$  being the energy monitor):

$$\delta E = \frac{E_{18}[2] + E_{18}[3]}{2} - \frac{E_{18}[0] + E_{18}[1]}{2}$$

The data should be distributed with a peak around 22,6 keV. To obtain the correct scaling factor for the values stored in the data tree we plot the voltage values measured by the ENMO monitor. 3 runs of data where taken with different Beam current, to study the dependence of the measured quantity from the beam current. From the mean of the distribution it is possible to estimate the scaling factor for the ENMO monitors, obtaining the physical quantity in the following way:

$$C_{E_{18}} = \frac{22,6 \text{ keV}}{\overline{\delta E}}$$

Taking the average over  $E_{18}$  voltage values, and using the formula above, we obtain the coefficient  $C_{E_{18}}$ . To take care of the current dependence of the monitors, the scaling factor to be placed in the standard.config

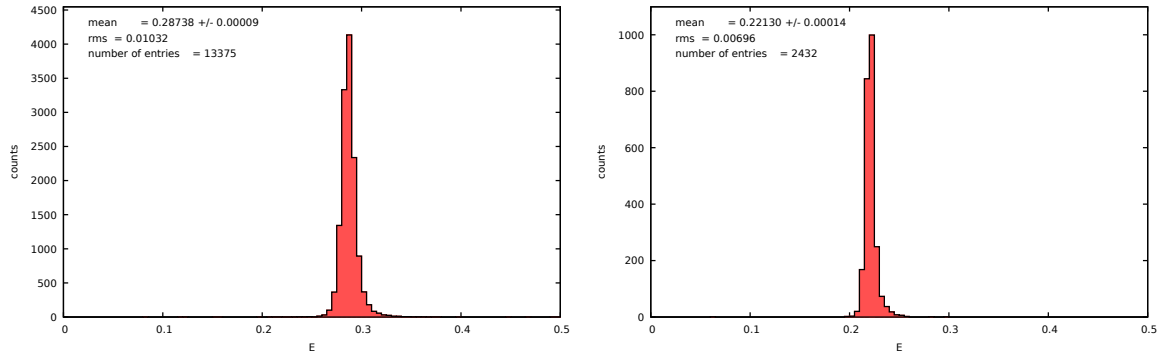


Figure 4.6:  $\delta E$  for 20 20  $\mu A$

file is:  $C_{E18}\bar{I}_{\mu A}$ . The calibration was performed taking three short acquisitions with different beam current : 20  $\mu A$ , 15  $\mu A$  and a run without beam.

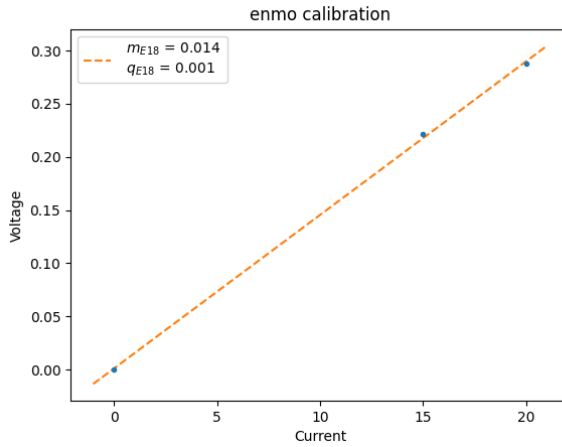


Figure 4.7: Calibration of ENMO monitor

From this we obtain the value  $scaling_{E18} = -1595.2$ , to obtain the physical quantity from the analysis. As a final check the final histogram for the physical quantity is shown:

#### 4.4.5 Calibration of the pmts

**Here it's important to show the plots I made during the beam time. I have to mention the Leo tecniques for the correct interpretation of counts vs attenuation.** During the beam time, several scans in attenuation were performed, before switching MAMI to produce the polarized beam, to choose the best working point for the PMTS of the detectors. The same procedure used in the laboratory was followed, starting from low attenuation and raising up the values. It's possible to get a simple model to describe the particular shape of the following plot taking into account simple assumptions about the type of electrical noise that affect the Nino board, and the *pdf* of the signal produced by the PMTS.

The main assumption ("this is not a true assumption, Anselm has a plot of the digitalize charge that proves that") is that the signal amplitude, in mV collected by the Nino board is well described by a gaussian distribution, and for signal with low amplitude, we expect to be well described by an uniform distribution. Just to visualize, let's suppose that the distribution of the signal amplitude collected is of this type (4.9) (the following figure is just an example, the values do not describe the data collected):

The probability for a signal to pass the selection is equal to the probability of being in above the threshold, that is the complementary cumulative of the gaussian distribution (probability of being in the right tail):

$$P(signal > thr) = 1 - \Phi(x) = \frac{1 - Erf(\frac{x_{thr} - x_0}{\sqrt{2}\sigma})}{2}$$

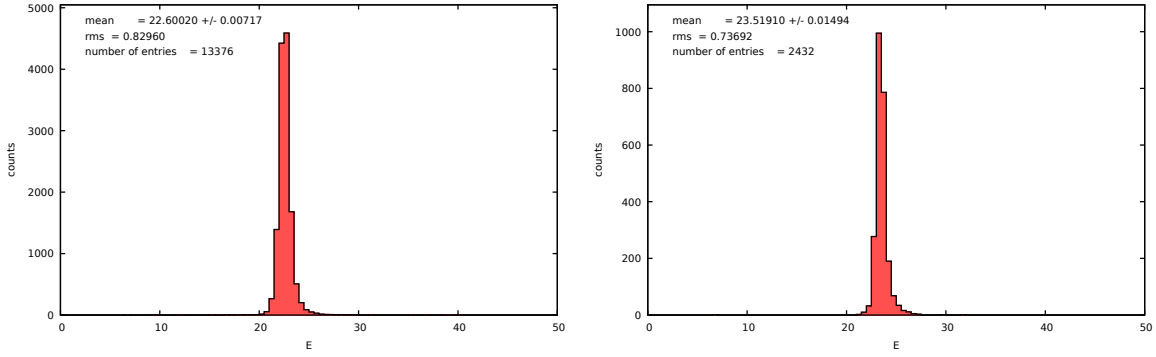


Figure 4.8: Plot for the physical quantities computed in the data tree, for two different current of the beam (on the left  $20 \mu\text{A}$ ,  $15 \mu\text{A}$  on the right)

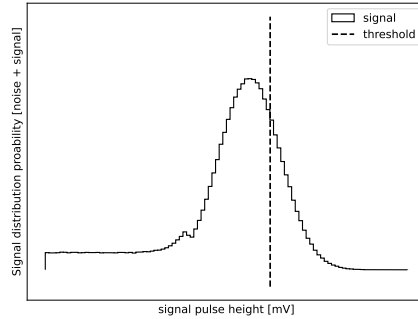


Figure 4.9: Example of the expected distribution of the PMTs output signal

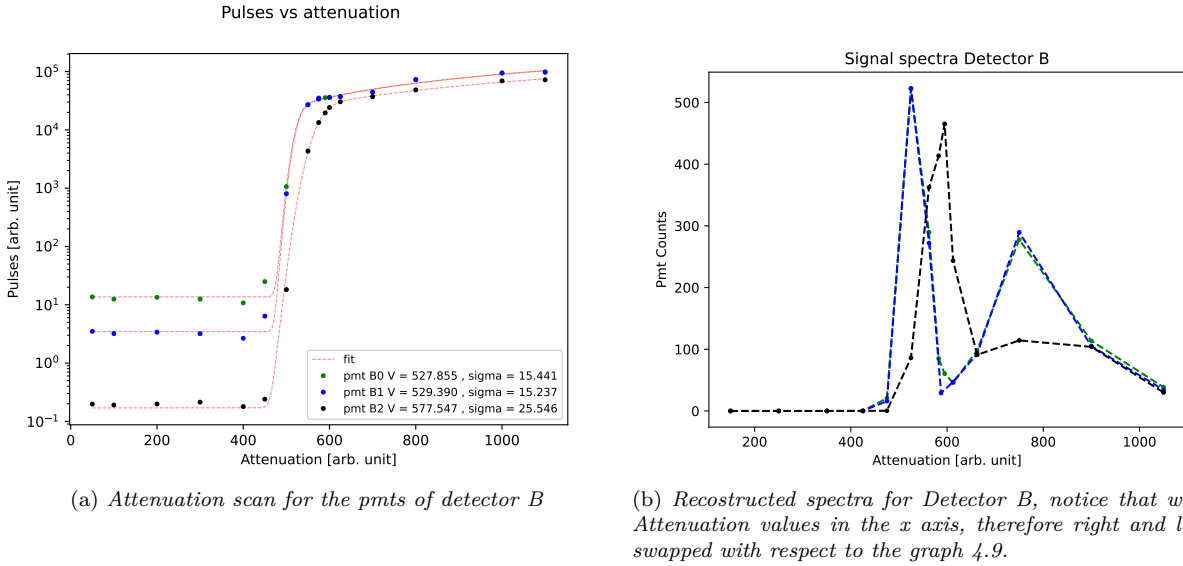
Once we reach the uniform zone, the probability of an even being selected is proportional to the area of the rectangle, which increases linearly decreasing the threshold. Considering the normalization factor, it is straightforward to fit the data with a model of this type:

$$N(\text{att}) = N_0 \cdot \frac{1 + \text{Erf}\left(\frac{x_{\text{thr}} - x_0}{\sqrt{2}\sigma}\right)}{2} \quad \text{if } \text{att} < C \\ N(\text{att}) = N(C) + m \cdot (\text{att} - C) \quad \text{if } \text{att} > C \quad (4.3)$$

For the detector B we show the result assuming our model:

From the fit we obtain three values for the signal Peak, given in attenuation units. We can check the idea behind this, visualizing the pmt count in a different way. In this plot (4.10a) there is a discrete differentiation of the data showed in (4.10b). This plot represents roughly the signal spectra of the signal. We can see that our assumption is not far from what we see, except for the fact that we are not able to identify the linear area. This is not very important, since we have to identify properly a good point to select all the real signals from the scattered electrons, rejecting the noise. Furthermore, if we look at the plot (), we can understand this behaviour looking that the threshold does not scale linearly with changing the attenuation value, for high values of attenuation, the threshold falls quickly at zero.

From the NINO documentation, it's possible to confront these values with



#### 4.4.6 Rates on lead

This section is straightforward. Basically I have to show the single plot of the pmts counts vs. beam current for lead target. However it's possible to do some preliminary studies, for example to calculate the time needed for measuring the asymmetry on lead with a certain error and maybe check from Mott cross section that the observed rate are fine.

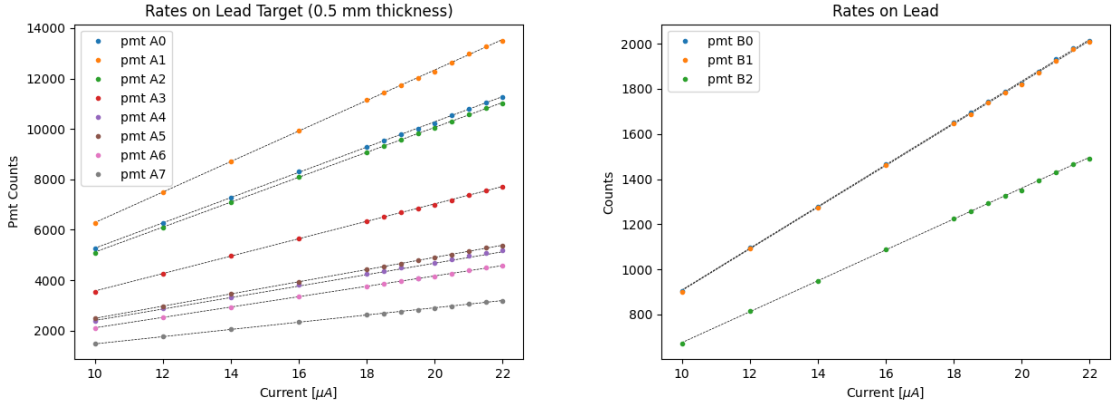


Figure 4.10: Rates on lead Target, for Detector A (left)

### 4.5 Asymmetry on Carbon

#### 4.5.1 Autocalibration procedure

#### 4.5.2 least square fit

When all the calibrations are performed, it is possible to proceed to generate the datafiles for the fit program. (spiegare in dettaglio come è fatto il programma di analisi)

For a better visualization of the data, especially to observe the dependence of the asymmetry on the Beam parameters measured, it is useful to take the average asymmetry at regular intervals. From the raw plots of the asymmetries (see below 4.11), it is clear that the statistical error associated to the asymmetry is the main one, and it's not possible to identify a linear dependence.

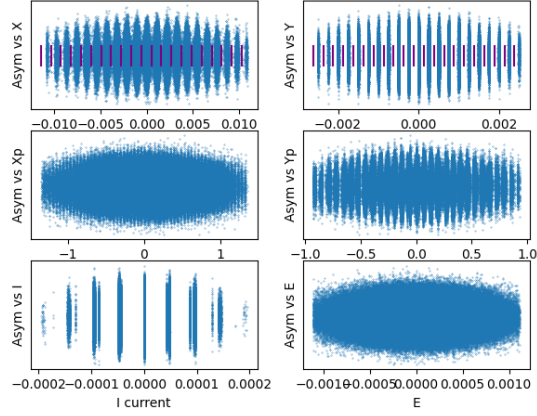
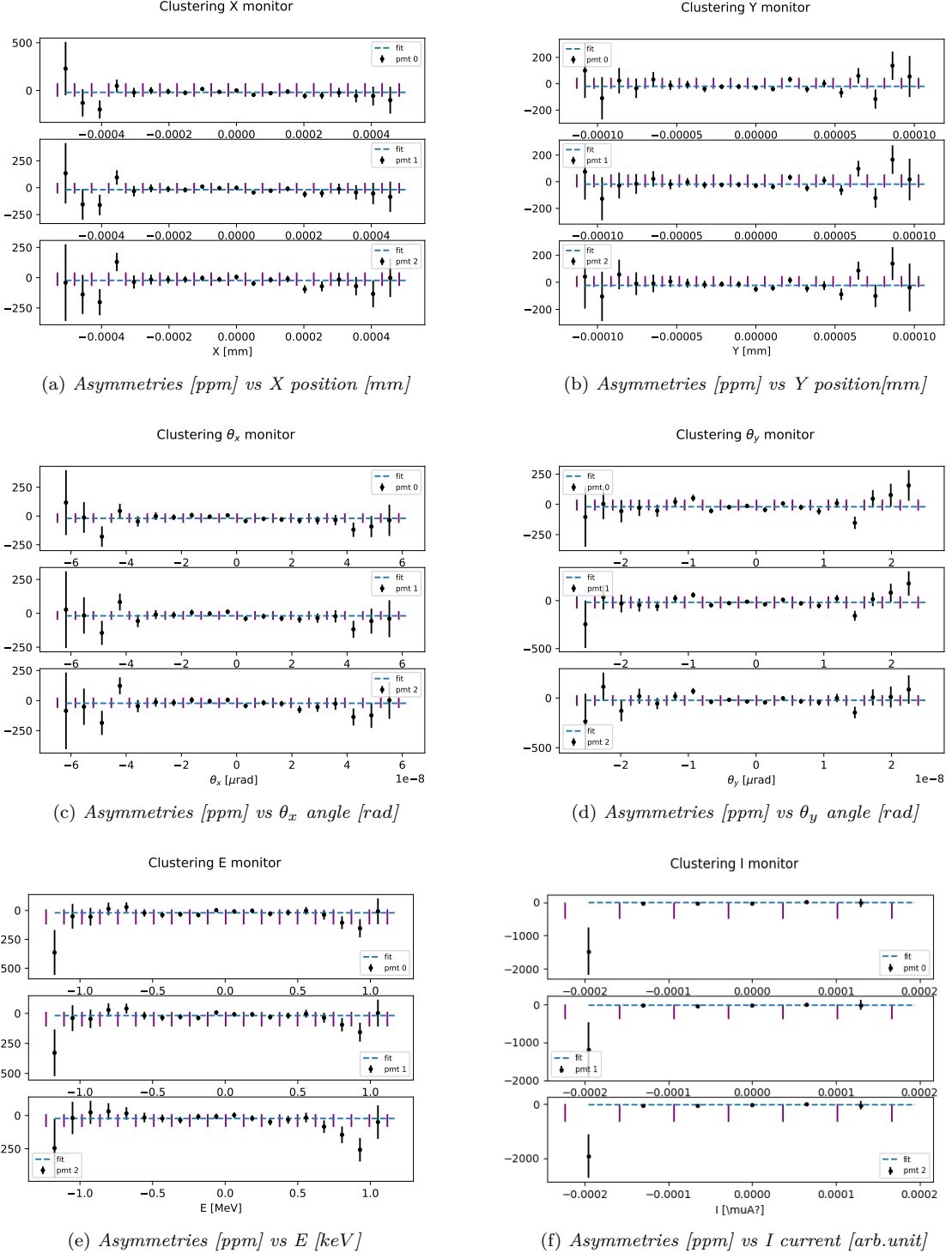


Figure 4.11: Asymmetries vs. Beam parameters

In some plots (X,Y and I) we can identify equally spaced cluster of data. So we decide to compute the averaged asymmetry for each cluster we were able to identify. In the following plots we decided to apply some cuts to the data, selecting only the events where the values of all the monitor are less then 3 standard deviation far from the mean. In all the figures the asymmetries are multiplied by a factor of 1e6 to have the result in ppm (so each y-axis is in ppm).

$$(x_{monitor} - \bar{x}_{monitor}) \leq 3 \cdot \sigma_X$$

For each monitor we use the *curve fit* function of the python library `scipy` to fit the data. Each Beam parameter is treated separately now, so in principle we are ignoring possible effect of correlation between the X-values (however, from the correlation matrix *write that somewhere* the effects are negligible)

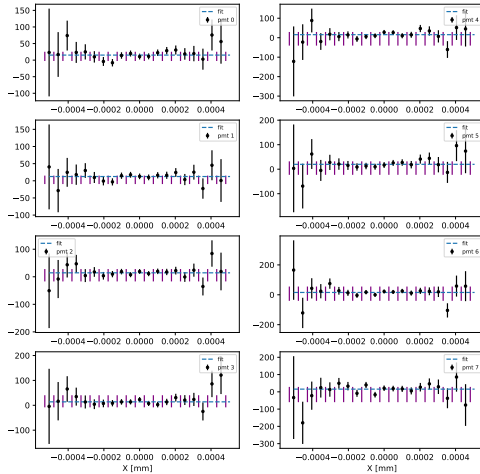


The error of each point is computed exploiting the same formula defined above (theory section;  $N_{A/B}$  averaged pmt counts for each subevents and  $n$  number of event in each interval):

$$\sigma_{Asym} = \frac{1}{\sqrt{2N_{A/B} \cdot n}}$$

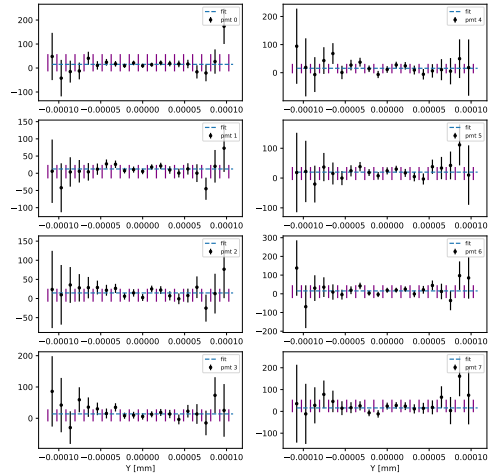
From this plots we can check if the linear model is good enough to describe the dependence of our data and decide if it should be useful to apply different cuts for certain beam parameters. We report now a first estimation of the false asymmetries, later the data will be fitted without treat separately the beam parameters. From that we can learn the effects of the correlation between the data.

Clustering X monitor



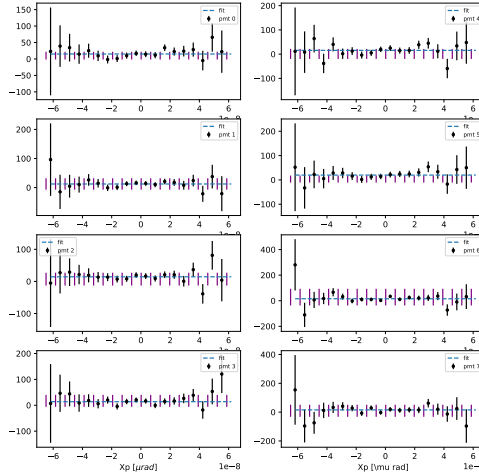
(a) Asymmetries [ppm] vs X position [mm]

Clustering Y monitor



(b) Asymmetries [ppm] vs Y position [mm]

Clustering Xp monitor

(c) Asymmetries [ppm] vs  $\theta_x$  angle [rad]

pmt:	B0	B1	B2	unit
$\frac{dA}{dX}$	$-66 \pm 37$	$-65 \pm 37$	$-80 \pm 47$	$\frac{\text{ppm}}{\mu\text{m}}$
$\frac{dA}{dY}$	$34 \pm 219$	$79 \pm 233$	$-213 \pm 219$	$\frac{\text{ppm}}{\mu\text{m}}$
$\frac{dA}{d\theta_y}$	$-416 \pm 1181$	$-443 \pm 1227$	$-1237 \pm 1130$	$\frac{\text{ppm}}{\mu\text{rad}}$
$\frac{dA}{d\theta_x}$	$-672 \pm 297$	$-672 \pm 307$	$-845 \pm 380$	$\frac{\text{ppm}}{\mu\text{rad}}$
$\frac{dA}{dE}$	$-0.004 \pm 0.016$	$-0.011 \pm 0.016$	$-0.044 \pm 0.018$	$\frac{\text{ppm}}{\text{keV}}$

#### 4.5.3 False asymmetries

Seems that is possible to obtain rough estimates of the beam related asymmetries with the results from the fit. For Energy and position it's achievable, while for the angles it's quite hard (in principle sounds possible to perform an analytic calculation of the asymmetry related to the incident beam angle, however Anselm told me that quite often those results are in disagreement with the observed even in the sign!).

Until now the values for the false asymmetries were treated as the parameters of the fit. In this section we will investigate how we can obtain another different estimations, useful to check the validity of all the process of analysis of the data.

For  $\frac{dA}{dX}$  and  $\frac{dA}{dY}$ , we conceptually exploit the possibility of varying the position of the beam on the target, as we did during one of the calibration phases. Using the same *wobbler 16* we asked MAMI to slowly change the beam position on the X and Y monitor. The change in position has the effect to modify the rates for the two detector, and from them it's possible to extract estimate the two false asymmetries related to the beam position. Now we will see how the two quantities are related.

From the plot ... we see that the counts are scaling linearly with the beam position, so we assume that the  $N$  are given by

$$N(x, \dots) = N_0 + m \cdot (x - x_0)$$

it is clear that the linear model can't be always good, at some point the electron will be deflected completely out of the detector, however for the small variation that the magnets are producing this can be assumed without risk. Then we can try to compute the asymmetry for two different beam position  $x_1$  and  $x_2$ :

$$Asym = \frac{N(x_1) - N(x_2)}{N(x_1) + N(x_2)} = \frac{N_0 + m \cdot (x_1 - x_0) - N_0 - m \cdot (x_2 - x_0)}{N(x_1) + N(x_2)} = \frac{m}{2N_0 + m \cdot (x_1 + x_2) - 2mx_0} (x_1 - x_2) \quad (4.4)$$

We can approximate the denominator deleting the term  $m \cdot (x_1 + x_2)$  which should be small compared to  $2N_0$ . We end with:

$$Asym = \frac{m}{2N_0 - 2mx_0} (x_1 - x_2) \quad (4.5)$$

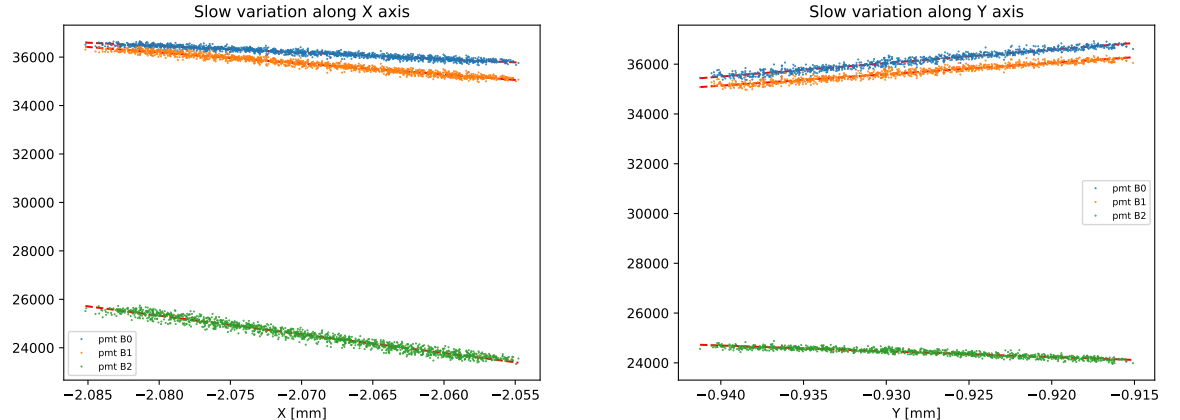
The term in front of  $(x_1 - x_2)$  can be compared to  $\frac{dA}{dX}$ .  $x_0$  is arbitrary and can be set to 0. For  $N_0$ , the offset, we substitute the averaged value counts of each pmt for the polarized beam acquisitions (we remind that the rate are collected during each 20 ms time interval of each sub-event).

The data are reported in the table below:

Pmt	Detector A	Detector B
pmt 0	84718	18925
pmt 1	96882	18815
pmt 2	80604	14807
pmt 3	65053	
pmt 4	45943	
pmt 5	46248	
pmt 6	37452	
pmt 7	25808	

We report the values obtained with this new method ...

We can investigate also the asymmetries related to the beam energy. For this one we can exploit the theoretical expression for the Mott cross-section, taking the derivative ...



(a) Plot for slow variation in  $x$  direction for detector  $B$ .

(b) Plot for slow variation in  $x$  direction for detector  $B$ .

#### 4.5.4 ??Bootstrap??

Although Anselm was against it, now seems possible to increase the precision of the measurement with a procedure similar to a bootstrap. Instead of computing all the quantities inside a single event, it's possible to compute all the important quantities also between different events. In this scenario the statistics can be increased artificially as much as we want, with the same amount of data. Of course, it's also simple to abuse of this method, so we should restrict using only events next to each other. However seem reasonable and promising.

#### 4.5.5 ??interval estimation??

## **Chapter 5**

# **Conclusion and outlook**

- result of the Analysis

# Appendices

## **Appendix A**

### **Some Appendix**

The contents...

# Bibliography

- [1] Single and multichannel, synchronous voltage-to-frequency converters, ad7741. *Analog Devices*.
- [2] B.S. Schlimme, P. Achenbach, K. Aulenbacher, S. Baunack, D. Bender, J. Beričič, D. Bosnar, L. Correa, M. Dehn, M.O. Distler, A. Esser, H. Fonvieille, I. Friščić, B. Gutheil, P. Herrmann, M. Hoek, S. Kegel, Y. Kohl, T. Kolar, H.-J. Kreidel, F. Maas, H. Merkel, M. Mihovilović, J. Müller, U. Müller, F. Nillius, A. Nuck, J. Pochodzalla, M. Schoth, F. Schulz, C. Sfienti, S. Širca, B. Spruck, S. Štajner, M. Thiel, V. Tioukine, A. Tyukin, and A. Weber. Vertical beam polarization at MAMI. *Nuclear Instruments and Methods in Physics Research Section A: Accelerators, Spectrometers, Detectors and Associated Equipment*, 850:54–60, apr 2017.